PLOS COMPUTATIONAL BIOLOGY

RESEARCH ARTICLE

Computational analysis of memory consolidation following inhibitory avoidance (IA) training in adult and infant rats: Critical roles of CaMKIIα and MeCP2

Yili Zhang[1], Paul Smolen[1], Cristina M. Alberini[2], Douglas A. Baxter[1,3], John H. Byrne[1]*

1 Department of Neurobiology and Anatomy; W.M. Keck Center for the Neurobiology of Learning and Memory; The University of Texas Medical School at Houston, Houston, Texas, United States of America, **2** Center for Neural Science, New York University, New York City, New York, United States of America, **3** Department of Neurobiology and Experimental Therapeutics, College of Medicine, Texas A&M University, Houston, Texas, United States of America

* John.H.Byrne@uth.tmc.edu

Citation: Zhang Y, Smolen P, Alberini CM, Baxter DA, Byrne JH (2022) Computational analysis of memory consolidation following inhibitory avoidance (IA) training in adult and infant rats: Critical roles of CaMKIIα and MeCP2. PLoS Comput Biol 18(6): e1010239. https://doi.org/10.1371/journal.pcbi.1010239

Editor: Joanna Jędrzejewska-Szmek, Instytut Biologii Doswiadczalnej im M Nenckiego Polskiej Akademii Nauk, POLAND

Received: January 5, 2022

Accepted: May 23, 2022

Published: June 27, 2022

Data Availability Statement: Source codes are submitted to the ModelDB database [46] (https://senselab.med.yale.edu/modeldb/ShowModel?model=267364#tabs-1, Access code: 123456) and to GitHub (https://github.com/YiliZhang8/BDNF-model-for-PLOS-Computational-Biology). XPPAUT files can be converted to Systems Biology Markup Language (SBML) files by SBML converters (see: https://sbmlutils.readthedocs.io/en/latest/).

Abstract

Key features of long-term memory (LTM), such as its stability and persistence, are acquired during processes collectively referred to as consolidation. The dynamics of biological changes during consolidation are complex. In adult rodents, consolidation exhibits distinct periods during which the engram is more or less resistant to disruption. Moreover, the ability to consolidate memories differs during developmental periods. Although the molecular mechanisms underlying consolidation are poorly understood, the initial stages rely on interacting signaling pathways that regulate gene expression, including brain-derived neurotrophic factor (BDNF) and Ca^{2+}/calmodulin-dependent protein kinase II α (CaMKIIα) dependent feedback loops. We investigated the ways in which these pathways may contribute to developmental and dynamical features of consolidation. A computational model of molecular processes underlying consolidation following inhibitory avoidance (IA) training in rats was developed. Differential equations described the actions of CaMKIIα, multiple feedback loops regulating BDNF expression, and several transcription factors including methyl-CpG binding protein 2 (MeCP2), histone deacetylase 2 (HDAC2), and SIN3 transcription regulator family member A (Sin3a). This model provides novel explanations for the (apparent) rapid forgetting of infantile memory and the temporal progression of memory consolidation in adults. Simulations predict that dual effects of MeCP2 on the expression of *bdnf*, and interaction between MeCP2 and CaMKIIα, play critical roles in the rapid forgetting of infantile memory and the progress of memory resistance to disruptions. These insights suggest new potential targets of therapy for memory impairment.

Funding: The study is supported by NIH grant NS102490 to (YZ, PS, JHB). https://grantome.com/grant/NIH/R01-NS102490-04 The study is also supported by NIH grant MH065635 to (CMA). https://grantome.com/grant/NIH/R37-MH065635-18 The funders had no role in study design, data collection and analysis, decision to publish, or preparation of the manuscript.

Competing interests: The authors have declared that no competing interests exist.

Author summary

Long-term memories (LTMs) are enduring and resistant to disruption. These features are acquired *via* processes collectively referred to as consolidation. In adults, the initial stages of consolidation follow complex dynamics that are believed to emerge from interacting biochemical signaling pathways, including BDNF and CaMKIIα dependent feedback loops. Similarly, the acquisition of ability to consolidate memory in infantile animals is believed to emerge from the functional maturation of these molecular pathways. Here, the ways in which these pathways contribute to consolidation were investigated using a computational model. This model provides novel explanations for the apparent rapid forgetting of infantile memory and for development of resistance to disruption during memory consolidation.

Introduction

The transformation of an initially fragile memory into a stable long-term memory (LTM) is known as consolidation and can require days to complete [1,2]. Zhang et al. [3] developed a computational model of a hippocampal brain-derived neurotrophic factor (BDNF)—cAMP response element-binding protein (CREB)-CCAAT-enhancer-binding protein (C/EBPβ) positive feedback loop activated by inhibitory avoidance (IA) training in rats. Simulations predicted that the dynamics of the BDNF-CREB-C/EBPβ feedback loop have a significant effect on consolidation of long-term IA memory. Here, the Zhang et al. [3] model was extended to include additional signaling cascades:

1. Regulation of Ca^{2+}/calmodulin-dependent protein kinase II alpha (CaMKIIα) is believed to be critical for the formation of IA memory. Based on empirical findings [4–6], a BDNF–CaMKIIα-BDNF feedback loop was included in the revised model.
2. The model adopted a 'dual operation mode' of regulation of BDNF by MeCP2 [7]. The effect of MeCP2 on *bdnf* expression has two components: activation by MeCP2 alone, and repression by a MeCP2 /HDAC2/Sin3a complex.

We used the revised model to gain insights into apparent rapid decay of infantile memory. In contrast to memories formed in adults that will be stable and long-lasting, infantile memories formed early during development are usually more labile in that they commonly are no longer expressed days after learning, although the latent memory trace may be reinstated by some specific protocols or artificial reactivation [8–11]. In the hippocampus, many proteins related to synaptic plasticity have different basal expression levels in infants *vs*. adults. In infantile rats, the basal level of phosphorylated CaMKIIα (pCaMKIIα) is substantially lower than that of adult rats, whereas the basal level of phosphorylated CREB (pCREB) is substantially higher than that of adult [12]. Our revised model simulates IA memory formation with different basal levels of pCaMKIIα and pCREB.

We also used the model to study the development of resistance to disruption during memory consolidation following IA training. The consolidation of memory is a process of developing resistance to disruption [1]. Initially, memory is vulnerable to protein synthesis inhibitors (PSIs), but it becomes resistant over time, hence at the later stage of consolidation. IA memory at 7 days after learning can be impaired by PSI applied at 24 h after learning, but becomes resistant to PSI applied at 48 h after learning [5]. Empirical and computational studies suggest self-sustained positive feedback loops contribute to synaptic plasticity and memory formation and consolidation [3, 5, 13–24]. After positive feedback is activated by learning, its strength

increases with time. Therefore, the later PSI is applied after learning, the more resistant is the positive feedback, and memory, to disruption [3].

However, resistance of memory to disruption does not always continuously grow with time post-learning. In Bekinschtein et al. [25], IA memory at day 7 was impaired by PSI added 12 h after training, but memory was resistant if PSI was added at earlier times. Some studies suggested that two distinct waves of protein synthesis during consolidation contribute to complex dynamics of resistance [25–27]. Zhang et al. [3] delayed the initiation of a BDNF feedback loop to generate two such waves, and consequent time windows of sensitivity to PSI. However, the time windows found in empirical studies show a large diversity and are to some extent contradictory [25–27]. These differences may, in part, occur because the large number of empirical variables (e.g., type of training, circadian rhythms, age, areas of the brain, animal) has made it difficult to consistently characterize the concept of a time window(s). The key mechanisms underlying the generation of distinct time windows are still poorly understood.

Due to these considerations, we did not aim to replicate any time windows found in empirical studies. Our model simulated the characteristic features of dynamics of BDNF, *bdnf*, pCREB, C/EBPβ and pCaMKIIα, and the binding of Sin3a/MeCP2/HDAC2 after IA training, as described in Bambah-Mukku et al. [5]. In this relatively biological realistic model, we simulated PSI effects, and investigated biochemical processes that may underlie both the overall increased resistance to PSI with time, and the observed temporary decrease of resistance during a particular period after PSI application.

Methods: Model development

The model of Zhang et al. [3] focused on the BDNF-CREB-C/EBPβ feedback loop in rat hippocampal neurons. In simulations, the feedback loop was initiated with a one-trial IA training-induced release of BDNF, which leads to rapid activation of the transcription factor CREB *via* phosphorylation, and a consequent increase in expression of the transcription factor C/EBPβ. Increased levels of C/EBPβ close the loop by increasing *bdnf* expression. We extended this model by adding several new components (Fig 1A):

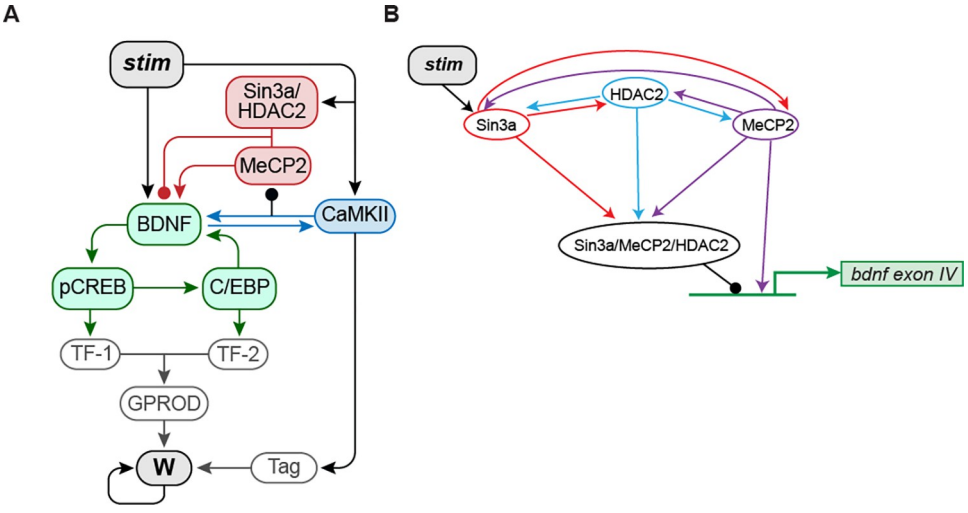

Fig 1. Schematic model of the signaling pathways essential to consolidation of IA long-term memory (LTM). (A) Signaling pathways with multiple feedback loops, including positive BDNF-CaMKIIα (blue) and BDNF-C/EBPβ (green) feedback loops that contribute to memory consolidation. MeCP2, HDAC2 and Sin3a bi-directionally regulate BDNF expression (red). Details and equations are given in the main text. (B) Scheme of interactions among bound Sin3a (red), MeCP2 (purple) and HDAC2 (blue), and their effects on the *bdnf* exon IV promoter. Arrowheads indicate activation, circular ends indicate repression.

https://doi.org/10.1371/journal.pcbi.1010239.g001

1. BDNF-CaMKIIα-BDNF positive feedback (Eqs 1, 8–10). Empirical studies indicate that active CaMKIIα, i.e., phosphorylated CaMKIIα (pCaMKII) in the rat hippocampus remains increased for at least 20 h after IA training [4,5]. The increase of pCaMKIIα is significantly reduced by anti-BDNF treatment [5], which in turn blocks memory formation [4], suggesting activation of CaMKIIα is at least partially dependent on BDNF and accompanies memory formation. pCaMKIIα, in turn, supports extracellular release of BDNF and long-term changes in dendritic structure at CA3-CA1 hippocampal synapses [6]. Together, these results suggest autocrine BDNF-TrkB-CaMKIIα-BDNF signaling is important for synaptic plasticity and memory formation in the dorsal hippocampus. Thus, we included a BDNF-CaMKIIα-BDNF positive feedback loop (Fig 1A). This loop does not require protein synthesis, thus the dynamics of this loop are faster compared to the BDNF-CREB-C/EBPβ feedback loop.

2. Binding of MeCP2, Sin3a, and HDAC2 to the *bdnf* promoter (Eqs 11–13). Modeling the dynamics of MeCP2, Sin3a, and HDAC2 binding to the *bdnf exon IV* promoter after IA training based on the empirical findings of Bambah-Mukku et al. [5] (Fig 1). After IA training, distinct dynamics were observed for the binding of Sin3a, MeCP2 and HDAC2. Binding of Sin3a significantly increased within 30 min and decreased at 12 h, followed by a second increase at 48 h. In contrast, binding of MeCP2 and HDAC2 remained near the basal level for at least 12 h after IA training, but significantly increased at 48 h.

3. Dual effects of MeCP2 on *bdnf* transcription (Eqs 5–7). The action of MeCP2 on *bdnf* expression was modeled with two components: a constitutive function representing up-regulation of basal *bdnf* expression by free MeCP2, and a dynamic function to represent down-regulation by a MeCP2/HDAC2/Sin3a complex (Fig 1). The effects of MeCP2 on gene expression are complex [28,29]. MeCP2 can act as a repressor or activator of BDNF transcription depending on context. In neurons, MeCP2 can act constitutively as a *bdnf* activator [30]. Constitutive MeCP2 overexpression enhances *bdnf* expression, and MeCP2 deletion inhibits *bdnf* expression [31]. Other studies suggest increased MeCP2 can act directly as a *bdnf* repressor [5, 32,33]. For example, termination of the BDNF positive feedback loop is associated with increased binding of MeCP2, HDAC2, and Sin3a to the *bdnf exon IV* promoter region at 48 h post IA training [5]. Li and Pozzo-Miller [7] proposed a "dual operation model" in which neuronal activity or other dynamical processes can switch the role of MeCP2 between activation and repression of *bdnf*. The association of MeCP2 with HDAC2–Sin3a could constitute such a switch component.

4. Downstream signaling cascades to mediate synaptic plasticity (Eqs 14–21). These were based on synaptic tagging and capture, which is critical for the formation of protein synthesis-dependent long-term potentiation and induction and consolidation of LTM [34–38].

Equations for CaMKIIα-dependent regulation of the BDNF -CREB -C/EBPβ pathway

Eqs 1–4 describe activation of the BDNF -CREB -C/EBPβ pathway after stimulation, modifed from those in Zhang et al. [3].

$$\frac{d[BDNF]}{dt} = r_{BDNF} stim + k_{fB} \frac{[pCaMKII]}{[pCaMKII] + K_{CaMKII,BDNF}} \frac{[bdnf]}{[bdnf] + K_{trans}} (1 - ANI) - k_{dBDNF} \frac{[BDNF]}{[BDNF] + K_{dB}} \quad (1)$$

In Eq 1, *stim* represents a stimulus that simulates IA training. *Stim* induces the initial

activation of the BDNF pathway during training [39]. *Stim* is 0 before and after training, and increases to 30 μM/s for 1 min to simulate training. [*BDNF*] represents the concentration of BDNF released *via stim* or a CaMKIIα-dependent cascade. Released BDNF binds TrkB receptors to activate CREB and CaMKIIα. Active CaMKIIα in turn helps release more BDNF. *ANI* (anisomycin) remains at 0 in the absence of PSI and increases to 0.8 for 6 h to simulate PSI, based on empirical findings [5, 40].

$$\frac{d[pCREB]}{dt} = (k_{basalp\_creb} + k_{phos\_creb}\frac{[BDNF]^2}{[BDNF]^2 + K_{CREB\_BDNF}{}^2})[CREB] - k_{dphos\_creb}[pCREB] \quad (2)$$

$$[CREB] = CREB_{total} - [pCREB] \quad (3)$$

$[CREB_{total}]$ is the concentration of total CREB (Eq 3). *[pCREB]* is phosphorylated CREB (pCREB) (Eq 2). Empirical studies indicate that total CREB remains at its basal level for 20 h after IA training in rat hippocampus, whereas pCREB remains increased for more than 24 hours returning to baseline by 48 h after training [4–5]. The increase of pCREB is blocked by anti-BDNF treatment [5], suggesting the activation of CREB depends on BDNF.

$$\frac{d[\mathrm{C/EBP}]}{dt} = \{(k_{basal\_cebp} + k_{f\_creb}\frac{[pCREB]^2}{[pCREB]^2 + K_{CREB\_CEBP}{}^2})(CEBP_{\max} - [C/EBP])(1 - ANI) - k_{d\_cebp}\frac{[C/EBP]}{[C/EBP] + K_{cebp}}\}/\tau_{cebp} \quad (4)$$

[C/EBP] is the total concentration of C/EBPβ protein (Eq 4). Hill functions with coefficient of 2 are used to describe the effect of pCREB on *c/ebp* expression and the effect of C/EBPβ on *bdnf* expression, based on data suggesting these transcription factors commonly function as dimers. pCREB significantly increases 30 min after IA training [5], whereas *c/ebp*β mRNA and C/EBPβ protein do not increase until hours after training [5, 41]. The mechanism underlying the slow response of C/EBPβ is unclear. In the revised model, the arbitrary suppression of the effect of pCREB on C/EBPβ expression implemented in Zhang et al. [3] was removed. The response of C/BEPβ to pCREB is assumed slow. The parameter τ_{cebp} in Eq 4 determines the speed of response of C/EBPβ to pCREB. τ_{cebp} was adjusted so that two waves of increase in the release of BDNF protein were induced after stimulus. The first was directly induced by stimulus, whereas the second was ~10 h after stimulus due to the activation of BDNF-C/EBPβ and BDNF-CaMKIIα feedback loops. C/EBP_{max} is the maximum amount of C/EBPβ that can be produced within 48 h as described in Zhang et al. [3].

Regulation of *bdnf* transcription by C/EBP, MeCP2, Sin3a, and HDAC2

Eqs 5–7 describe the regulation of *bdnf* transcription by various factors. Eq 5 is modified from the model of Zhang et al.[3]. Eqs 6 and 7 are new equations.

$$\frac{d[bdnf_m]}{dt} = k_{b\_MeCP2}(1 + [E_{MeCP2}]) + k_{f\_bdnf}\frac{[CEBP]^2}{K_{a\_bdnf}{}^2 + [CEBP]^2 + [E_{Comp}]^2} - k_{\mathrm{deg}b}\frac{[bdnf_m]}{[bdnf_m] + K_{db}} \quad (5)$$

$$\frac{d[E_{MeCP2}]}{dt} = \{k_{f\_EMeCP2}\frac{[B_{MeCP2}] - [B_{MeCP2}]_{basal}}{[B_{\mathrm{Sin3}a}][B_{HDAC2}]}([E_{MeCP2}]_{\max} - [E_{MeCP2}]) - [E_{MeCP2}]\}/\tau_{E\_MeCP2} \quad (6)$$

$$\frac{d[E_{Comp}]}{dt} = \{k_{f\_comp}([B_{MeCP2}] - [B_{MeCP2}]_{basal})([B_{\mathrm{Sin3a}}] - [B_{\mathrm{Sin3a}}]_{basal}) \\ ([B_{HDAC2}] - [B_{HDAC2}]_{basal})([E_{Comp}]_{\max} - [E_{Comp}]) - k_{d\_comp}[E_{Comp}]\}/\tau_{Comp} \quad (7)$$

Transcription of *bdnf* is regulated by the activator C/EBPβ and three repressors: Sin3a, MeCP2, and HDAC2 [5]. In Eq 5, the expression of *bdnf* mRNA is activated by [*C/EBP*], whereas *bdnf* is repressed by the effect of the Sin3a/MeCP2/HDAC2 complex, represented by the variable $[E_{comp}]$ ('*E*' representing 'effect'; '*comp*' representing 'complex'). $[E_{comp}]$ increases due to increased binding of Sin3a ($[B_{sin3a}]$), MeCP2 ($[B_{MeCP2}]$), and HDAC2 ($[B_{HDAC2}]$) (Eq 7).

The effect of free MeCP2 on expression of *bdnf* is represented by $[E_{MeCP2}]$ (Eq 5) (here '*MeCP2*' represents free MeCP2 unbound to Sin3a or HDAC2). When the binding of MeCP2 to *bdnf exon IV* promoter is at the basal level, the basal translation rate is k_{b_MeCP2}. Overexpression or deletion of MeCP2 will increase or decrease $[E_{MeCP2}]$, respectively. $[E_{MeCP2}]$ increases with increased binding of MeCP2 alone ($[B_{MeCP2}]$ in Eq 6) but decreases with increased binding of Sin3a ($[B_{Sin3a}]$) and HDAC2 ($[B_{HDAC2}]$), which bind MeCP2 to form the inhibitory Sin3a/MeCP2/HDAC2 complex (Eq 6) (Fig 1B). τ_{E_MeCP2} and τ_{Comp} are time constants governing how fast MeCP2 alone or MeCP2/Sin3a/HDAC2 complex respectively activate or repress the expression of *bdnf*.

Equations for CaMKIIα regulation by BDNF

Eqs 8–10 are new equations describing regulation of CaMKIIα. Empirical studies indicate that total CaMKIIα remains at its basal level after IA training in rat hippocampus, whereas pCaMKIIα is elevated for more than 24 h, returning to baseline by 48 h after training [4,5]. The increase of pCaMKIIα is significantly reduced by anti-BDNF treatment [5], suggesting this activation of CaMKIIα is dependent on BDNF (Eq 8). However, pCaMKIIα is also increased earlier, 30 min after IA training, and this early increase is not reduced by anti-BDNF treatment [5]. Thus, in the model, *stim* in Eq 8 is used to directly increase [*pCaMKII*] immediately after training. Also, the increase in pCaMKIIα at 12 h is not completely blocked by anti-BDNF treatment, which might be due to self-sustaining autophosphorylation of CaMKIIα [22, 42].

$$\frac{d[pCaMKII]}{dt} = (r_{CaMKII}stim + k_{basalp\_CaMKII} + E_{feedback})[CaMKII] - k_{dphos\_creb}[pCaMKII] \quad (8)$$

$$[CaMKII] = pCaMKII_{total} - [pCaMKII] \quad (9)$$

$$E_{feedback} = k_{CaMKII\_B}\frac{[BDNF]^2}{[BDNF]^2 + K_{CaMKII\_BDNF}{}^2} + k_{CaMKII\_F}\frac{[pCaMKII]^2}{[pCaMKII]^2 + K_{CaMKII\_feed}{}^2} \quad (10)$$

Equations describing the dynamics of Sin3a, MeCP2 and HDAC2 binding

Eqs 11–13 are new equations describing the binding of Sin3a, MeCP2 and HDAC2 to the *bdnf exon IV* promoter. Binding of MeCP2 does not significantly increase until 48 h after IA training [5], an effect that may be due to pCaMKIIα [43]. pCaMKIIα can phosphorylate MeCP2 on S421, decreasing binding of MeCP2 to methylated DNA [43]. The binding of Sin3a increases within 30 min after IA training [5]. The mechanisms underlying the changes in binding of Sin3a, MeCP2 and HDAC2 to the *bdnf* exon *IV* promoter are unclear. In the model, *stim* in Eq 11 is used to directly increase $[B_{sin3a}]$ (the amount of bound Sin3a, Eq 6) after training (Fig

1B). Binding of Sin3a decreases at 12 h after IA training, followed by a second increase at 48 h, along with binding of MeCP2 and HDAC2. We hypothesize these similarities in binding dynamics reflect concurrent binding of Sin3a, MeCP2, and HDAC2 to form the Sin3a/MeCP2/HDAC2 complex. Thus increasing the binding of any two components (e.g., $[B_{MeCP2}]$ and $[B_{sin3a}]$) will increase binding of the third (i.e., $[B_{HDAC2}]$) (Eqs 12, 13) (Fig 1B). $[B_{Sin3a}]_{\max}$, $[B_{MeCP2}]_{\max}$ and $[B_{HDAC2}]_{\max}$ represent the maximal binding of these components.

$$\frac{d[B_{\mathrm{Sin3}a}]}{dt} = ((r_{\mathrm{sin3}a}stim + k_{f\_\mathrm{Sin3}a}[B_{MeCP2}][B_{HDAC2}])([B_{\mathrm{Sin3}a}]_{\max} - [B_{\mathrm{Sin3}a}]) - [B_{\mathrm{Sin3}a}])/\tau_{\mathrm{sin}a} \quad (11)$$

$$\frac{d[B_{HDAC2}]}{dt} = (k_{f\_HDAC2}[B_{MeCP2}][B_{\mathrm{Sin3}a}]([B_{HDAC2}]_{\max} - [B_{HDAC2}]) - [B_{HDAC2}])/\tau_{HDAC2} \quad (12)$$

$$\frac{d[B_{MeCP2}]}{dt} = (k_{f\_MeCP2}[B_{HDAC2}][B_{\mathrm{Sin3}a}]([B_{MeCP2}]_{\max} - [B_{MeCP2}]) - k_{d\_MeCP2}\frac{[pCaMKII]^2}{[pCaMKII]^2 + K_{pCaMKII\_MeCP2}{}^2}[B_{MeCP2}])/\tau_{MeCP2} \quad (13)$$

Equations describing the synaptic tagging and capture system

Eqs 14–21 are new equations describing the downstream synaptic tagging and capture system. These equations are adapted from [34, 44]. CaMKIIα activates a synaptic tag (Tag) in Eq 14. Tag is required for synaptic 'capture' of protein synthesized from a generic gene (GPROD in Eq 17) necessary for synaptic strengthening and LTM. Phosphorylated CREB activates a generic transcription factor TF-1 (Eq 15), whereas C/EBPβ activates a second transcription factor TF-2 (Eq 16) (Fig 1A). The rate of synthesis of GPROD, assumed necessary for synaptic strengthening, increases with TF-1 and TF-2 activation (Eq 17) (Fig 1A). The rate of increase of a synaptic weight W (Eqs 18–20) is determined by the product of Tag and GPROD (Fig 1A). The model simulates long-term synaptic potentiation (LTP) (increases in W, corresponding to formation of LTM) but does not currently simulate long-term synaptic depression (LTD). Thus, regulation of W is modeled by increasing W when the product of GPROD and Tag increases above its basal level. A Heaviside function, denoted as $()^+$, is used to represent regulation by Tag and GPROD (Eq 21). When the product of Tag and GPROD is below a basal level, $[Tag]_{basal}\ x\ [GPROD]_{basal}$, Tag and GPROD do not affect W.

$$\frac{d[Tag]}{dt} = (k_{f\_tag}[pCaMKKII](1 - [Tag]) - k_{d\_tag}[Tag])/\tau_{Tag} \quad (14)$$

$$\frac{d[TF-1]}{dt} = k_{f\_tif1}[pCREB](1 - [TF-1]) - k_{d\_tif1}[TF-1] \quad (15)$$

$$\frac{d[TF-2]}{dt} = k_{f\_tif2}[C/EBP](1 - [TF-2]) - k_{d\_tif2}[TF-2] \quad (16)$$

$$\frac{d[GPROD]}{dt} = ((k_{basal\_GROP} + k_{f\_GROD}\frac{[TF-1]}{[TF-1] + K_{tif1}}\frac{[TF-2]}{[TF-2] + K_{tif2}}) - k_{d\_GROD}[GPROD])/\tau_{GPROD} \quad (17)$$

$$\frac{d[W]}{dt} = ((k_{basal\_p} + k_{f\_w}E_{upstream})\frac{[P]}{[P] + K_p} - k_{d\_w}[W])/\tau_p \quad (18)$$

$$\frac{d[P]}{dt} = ([PP] - (k_{basal\_p} + k_{f\_w}E_{upstream})\frac{[P]}{[P] + K_p} - k_{d\_w}[P])/\tau_p \quad (19)$$

$$\frac{d[PP]}{dt} = (k_{f\_pp}\frac{[W]^2}{[W]^2 + K_{w\_pp}{}^2} - [PP])/\tau_{pp} \quad (20)$$

$$E_{upstream} = ([Tag][GPROD] - [Tag]_{basal}[GPROD]_{basal})([Tag][GPROD] - [Tag]_{basal}[GPROD]_{basal})^+ \quad (21)$$

so that

$E_{upstream} = [Tag][GPROD] - [Tag]_{basal}[GPROD]_{basal}$ when $[Tag][GPROD] - [Tag]_{basal}[GPROD]_{basal} > 0$

$E_{upstream} = 0$ when $[Tag][GPROD] - [Tag]_{basal}[GPROD]_{basal} <= 0$

As in Smolen et al. [34, 44], the increase in W is also assumed to be limited by the availability of a precursor molecule P (Eq 19). Moreover, in the current model, as a reactivating mechanism to maintain persistent memory (> 7 days), a simple positive feedback loop in which increased W tends to favor further growth, or stabilization, of W [22] is implemented. Increased W is assumed to feed back to increase the availability of P, through an intermediate pathway represented by PP (Eqs 20, 19). This feedback can allow W to remain at 200% or higher of its unstimulated (basal) value, a threshold set in Zhang et al. [3]. Long-term memory is assumed to be consolidated if W remains at least 200% or higher of its basal value for more than 2 days.

The parameter values in Table 1 were adjusted so that the model replicated the characteristic features of dynamics of BDNF, *bdnf*, pCREB, C/EBPβ and pCaMKIIα, and the binding of Sin3a/MeCP2/HDAC2 after IA training, as described in Bambah-Mukku et al. [5], and also maintained W higher than 200% control to simulate IA memory consolidation (Table 1).

Numerical methods

Fourth-order Runge-Kutta integration was used for integration of all differential equations with a time step of 3 s. Further time step reduction did not lead to significant improvement in accuracy. The steady-state levels of variables were determined after at least two simulated days, prior to any manipulations. The model was programmed in XPPAUT, a generally used numerical tool for simulating, visualizing and analyzing dynamical systems. It can be installed in various operating systems (http://www.math.pitt.edu/~bard/xpp/xpp.html) [45]. Source codes are submitted to the ModelDB database [46] (https://senselab.med.yale.edu/modeldb/ShowModel?model=267364#tabs-1, Access code: 123456) and to GitHub (https://github.com/YiliZhang8/BDNF-model-for-PLOS-Computational-Biology). XPPAUT files can be converted to Systems Biology Markup Language (SBML) files by SBML converters (see: https://sbmlutils.readthedocs.io/en/latest/).

Results

Simulated variations of W following IA training with altered CaMKIIα and CREB basal activities

Memories formed early during development are usually more labile in that they commonly are no longer expressed days after learning, although the latent memory trace may be reinstated

Table 1. Standard parameter values.

Parameter name	Value
r_{BDNF}	0.3 s^{-1}
k_{fB}	1.5 x 10^{-3} mM/s
$K_{CaMKII,BDNF}$	7.3 x 10^{-3} mM
K_{trans}	3 x 10^{-2} mM
K_{dB}	0.6 mM
k_{dBDNF}	6.6 x 10^{-4} mM/s
k_{basalp_creb}	3.2 x 10^{-6} s^{-1}
k_{dphos_creb}	9.6 x 10^{-5} s^{-1}
k_{phos_creb}	4 x 10^{-3} s^{-1}
K_{CREB_BDNF}	2 mM
$CREB_{total}$	0.085 mM
k_{basal_cebp}	1.6 x 10^{-2} s^{-1}
k_{f_cebp}	2.2 s^{-1}
k_{d_cebp}	5.7 x 10^{-3} mM/s
K_{CREB_CEBP}	0.19 mM
$CEBP_{max}$	2.3 x 10^{-1} mM
K_{cebp}	7.6 x 10^{-2} mM
τ_{cebp}	3 x 10^{3} s
k_{b_MeCP2}	1.6 x 10^{-7} mM/s
k_{f_bdnf}	1.6 x 10^{-4} mM/s
K_{a_bdnf}	3.2 mM
k_{degb}	4.5 x 10^{-5} mM/s
K_{db}	0.6 mM
k_{f_EMeCP2}	0.34 mM
$[E_{MeCP2}]_{\max}$	5 mM
τ_{E_MeCP2}	1.44 x 10^{4} s
k_{f_comp}	4.5 mM
k_{d_comp}	6.7 x 10^{-3} mM
$[B_{\mathrm{Sin3}a}]_{basal}$	1 mM
$[B_{HDAC2}]_{basal}$	1 mM
$[I_{Comp}]_{\max}$	5 mM
τ_{Comp}	3.6 x 10^{4} s
r_{CaMKII}	0.15 s^{-1}
k_{basalp_CaMKII}	3.6 x 10^{-6} mM/s
k_{dphos_CaMKII}	1.1 x 10^{-4} s^{-1}
$\rho CaMKII_{total}$	0.085 mM
k_{CaMKII_B}	5.3 x 10^{-5} mM/s
K_{CaMKII_BDNF}	0.28 mM
k_{CaMKII_F}	4.1 x 10^{-5} mM/s
K_{CaMKII_feed}	0.03 mM
$r_{\mathrm{sin}3a}$	3 x 10^{4} mM^{-1}
$k_{f\_\mathrm{Sin}3a}$	0.25 mM^{-2}
$\tau_{\mathrm{sin}a}$	5 x 10^{4} s
$[B_{\mathrm{Sin}3a}]_{\max}$	5 mM
k_{f_HDAC2}	0.25 mM^{-2}
$[B_{HDAC2}]_{\max}$	5 mM
τ_{HDAC2}	1.25 x 10^{5} s

(*Continued*)

Table 1. (Continued)

Parameter name	Value
k_{f_MeCP2}	0.25 mM^{-2}
$[B_{MeCP2}]_{max}$	5 mM
k_{d_MeCP2}	4 mM
$K_{pCaMKII\_MeCP2}$	0.011 mM
τ_{MeCP2}	1 x 10^4 s
k_{f_tag}	0.5 $mM^{-1}s^{-1}$
k_{d_tag}	0.03 s^{-1}
τ_{Tag}	5 s
k_{f_tif1}	1.1 x 10^{-4} $mM^{-1}s^{-1}$
k_{d_tif1}	3 x 10^{-5} s^{-1}
k_{f_tif2}	2.4 x 10^{-5} $mM^{-1}s^{-1}$
k_{d_tif2}	6 x 10^{-5} s^{-1}
k_{basal_GROP}	4 x 10^{-4} mM/s
k_{f_GROD}	7.5 mM/s
k_{d_GROD}	0.05 s^{-1}
K_{tif1}	1 mM
τ_{GPROD}	2 x 10^3 s
K_{tif2}	1 mM
k_{basal_p}	0.48 mM
k_{f_w}	1680 mM
K_p	13.3 mM
k_{d_w}	0.08 s^{-1}
$[tag]_{basal}$	0.1 mM
$[GPROD]_{basal}$	0.12 mM
K_{w_pp}	0.9 mM
τ_p	2.5 x 10^4 s
τ_{pp}	7.5 x 10^5 s
k_{f_pp}	0.8 mM

https://doi.org/10.1371/journal.pcbi.1010239.t001

by some specific protocols [8–9, 12]. This lability is thought to be linked to infantile amnesia, the inability of adults to remember infantile experiences. Although multiple hypotheses have been proposed [8–10, 12, 47,48], the mechanisms of rapid forgetting of infantile memory and reinstatement of latent memory traces remain unclear. Travaglia et al. [12] point out some of the substantial differences in biological systems of developing and adult brains. In the dorsal hippocampus of infantile rats, the basal level of pCaMKIIα is substantially lower than that of adult rats, whereas the basal level of pCREB is substantially higher than in adult [12]. To simulate the effects of these changes on the consolidation of IA memory, we gradually increased the basal phosphorylation rate of CREB, k_{basalp_creb} in Eq 2, from 100% of its standard value in Table 1 to ~300%, by steps of 20%. At the same time, we gradually decreased the basal phosphorylation rate of CaMKIIα, k_{basalp_CaMKII} in Eq 8, from 100% of its standard value in Table 1 to 50%, by steps of 10% (arrows in Fig 2A1). In all cases we first simulated several days of stimulus absence until the model reached a new equilibrium, and then simulated how these parameter changes affect the response to a stimulus. Basal binding of MeCP2, Sin3a and HDAC2 to the *bdnf* exon *IV* promoter was increased compared to control, due to the reduced basal pCaMKIIα, releasing its inhibition of MeCP2 binding. The increase in MeCP2 subsequently increased the binding of Sin3a and HDAC2. Fig 2A2 summarizes the results of these simulations with a 3-D plot of synaptic weight W as a function of both parameters k_{basalp_CaMKII} and

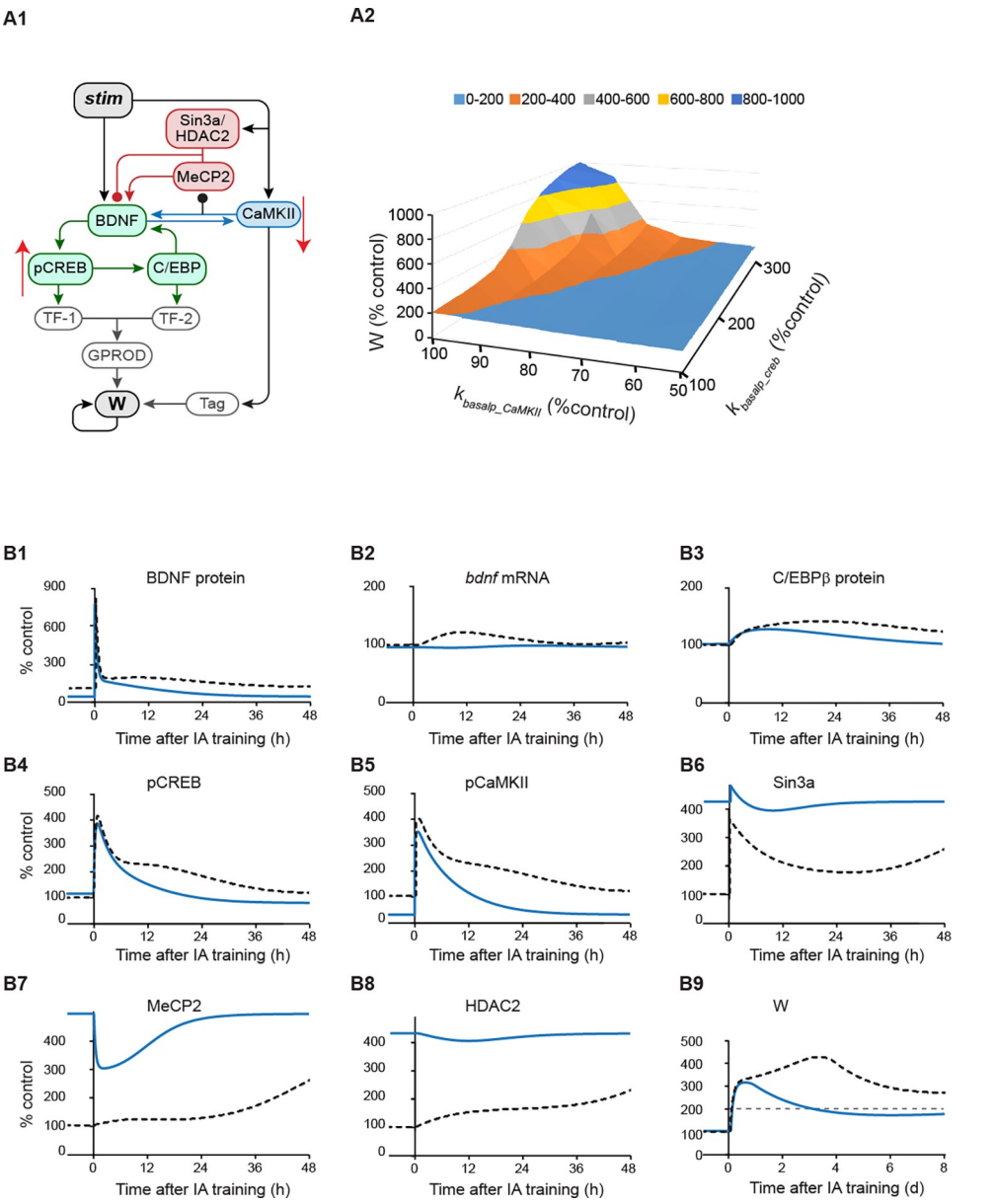

Fig 2. Simulated effects of increased pCREB combined with decreased pCaMKIIα on time courses of molecular pathways and synaptic weight W after IA training. (A1) Modifications of the model of the molecular pathways for IA conditioning, including increased basal phosphorylation of CREB, k_{basalp_creb}, concurrent with decreased basal phosphorylation of CaMKIIα, k_{basalp_CaMKII} (red arrows). (A2) 3D plot of synaptic weight W at day 7 after training with k_{basalp_creb} increasing from the standard value in Table 1 to 300% of the standard value, and k_{basalp_CaMKII} decreasing from the standard value in Table 1 to 50% of the standard value, with increased binding of MeCP2, Sin3a and HDAC2 (A2). The light blue area represents W less than 200% of basal level. (B) Example of dynamics of BDNF protein/mRNA (B1-2), C/EBPβ protein (B3), pCREB (B4), pCaMKIIα (B5), Sin3a binding (B6), MeCP2 binding (B7), HDAC2 binding (B8), and W (B9), with the standard parameter values in Table 1 (black dashed) or with k_{basalp_creb} increased by ~50% and k_{basalp_CaMKII} decreased by ~50% from control combined with higher binding levels of MeCP2, Sin3a and HDAC2 (blue) to simulate IA conditioning in infant rats. Gray dashed line in (B9) represents W at 200% control.

https://doi.org/10.1371/journal.pcbi.1010239.g002

k_{basalp_creb}. The light blue area represents W lower than 200% of basal level. Starting from the control simulation using the standard values of k_{basalp_creb} and k_{basalp_CaMKII} in Table 1, if the basal phosphorylation rate of CaMKIIα was reduced by more than 40%, *W* at day 7 always fell

below the 200% threshold that represents consolidated LTM, even if k_{basalp_creb} was substantially increased by more than 100% (light blue area, Fig 2A2). These simulations suggest that decreased pCaMKIIα in infant animals plays a role in the rapid forgetting of infantile memory.

Fig 2B illustrates an example of a simulation when the basal phosphorylation rate of CaMKIIα was decreased by ~50% and the basal phosphorylation rate of CREB was increased by ~50%, relative to control values (Table 1) to simulate IA conditioning in infant rats. Due to the decrease of basal pCaMKIIα prior to stimulus, releasing its inhibitory effect on MeCP2 binding; MeCP2, Sin3a and HDAC2 binding were all increased to higher basal levels compared to the control simulation (Fig 2B6–2B8, blue *vs*. black curves). Because of the higher level of bound MeCP2/Sin3a/HDAC2 complex, BDNF protein and *bdnf* mRNA remained lower than in the control simulation using the standard values of k_{basalp_creb} and k_{basalp_CaMKII} in Table 1 (Fig 2B1–2B2, blue *vs*. black-dashed curves), and the BDNF- C/EBPβ feedback loop was not fully activated after stimulus (Fig 2B1–2B4, blue *vs*. black-dashed curves). W only transiently increased, passing the threshold of 200%, but decreasing to below threshold at day 7 (Fig 2B9, blue *vs*. black-dashed curves). Taken together, these simulations suggest that enhanced binding of a MeCP2, Sin3a and HDAC2 complex to the *bdnf exon IV* promoter, caused by decreased pCaMKIIα in infant animals, might contribute to rapid forgetting of infantile memory. On the other hand, W did not return to the basal level at day 7 (Fig 2B9), which suggests that the memory trace is not completely lost, leaving the possibility of memory reinstatement at later times by specific protocols.

The current model cannot produce bistability (i.e., two steady states for the values of dynamic variables, with an appropriate perturbation switching between steady states). Bistability does not exist because the BDNF-dependent positive feedback loop is turned off, in the model, by the MeCP2/SIN3a/HDAC2 inhibitory complex at ~48 h after IA training, as suggested in Bambah-Mukku et al. [5]. However, to investigate a possible role of CaMKIIα in bistability, we blocked the effects of MeCP2, SIN3a, and HDAC2 on BDNF expression (S1A Fig). In this case, a bistable switch was induced by a transient stimulation. BDNF, *bdnf*, pCREB, pCaMKIIα, and C/EBP were all increased to a higher steady state after training (S1B Fig, blue curves). We then repeated the simulations in Fig 2, by gradually decreasing the basal phosphorylation rate of CaMKIIα, k_{basalp_CaMKII} in Eq 8, from 100% of its standard value in Table 1 to 10%, by steps of 10%. Concurrently, we gradually increased the basal phosphorylation rate of CREB, k_{basalp_creb} in Eq 2, from 100% of its standard value in Table 1 to ~300%, by steps of 20%. In all cases we examined whether these parameter changes would block the bistable switch of the above variables from the lower steady states to higher steady states after stimulation. We found that if k_{basalp_CaMKII} was decreased to 40% or less of its standard value, and k_{basalp_creb} was less than 140% of its standard value, the bistable switch was blocked. BDNF, *bdnf*, pCREB, pCaMKIIα, and C/EBP remained at the lower steady states at 48 h after IA training (S1C Fig). The simulation results with this model variant suggest that lower basal levels of pCaMKIIα in infant rats could suppress any potential bistability that might otherwise contribute to memory retention.

Simulated dynamics of resistance of W to protein synthesis inhibition (PSI)

The model replicated the characteristic features of dynamics of BDNF, *bdnf*, pCREB, C/EBPβ and pCaMKIIα, and the binding of Sin3a/MeCP2/HDAC2 after IA training, as described in Bambah-Mukku et al. [5]. Based these simulated time courses, we simulated dynamics of resistance of W to protein synthesis inhibition (PSI). Injection of the PSI anisomycin into rat dorsal hippocampus blocks >80% of protein synthesis for up to 6 h [5,40]. Thus, we reduced the synthesis rates of BDNF, C/EBP, TF1, TF2, GPROD and W by 80% for 6 h to simulate PSI (Fig 3A1, red Xs). To investigate the dynamics of memory resistance with respect to the time of PSI

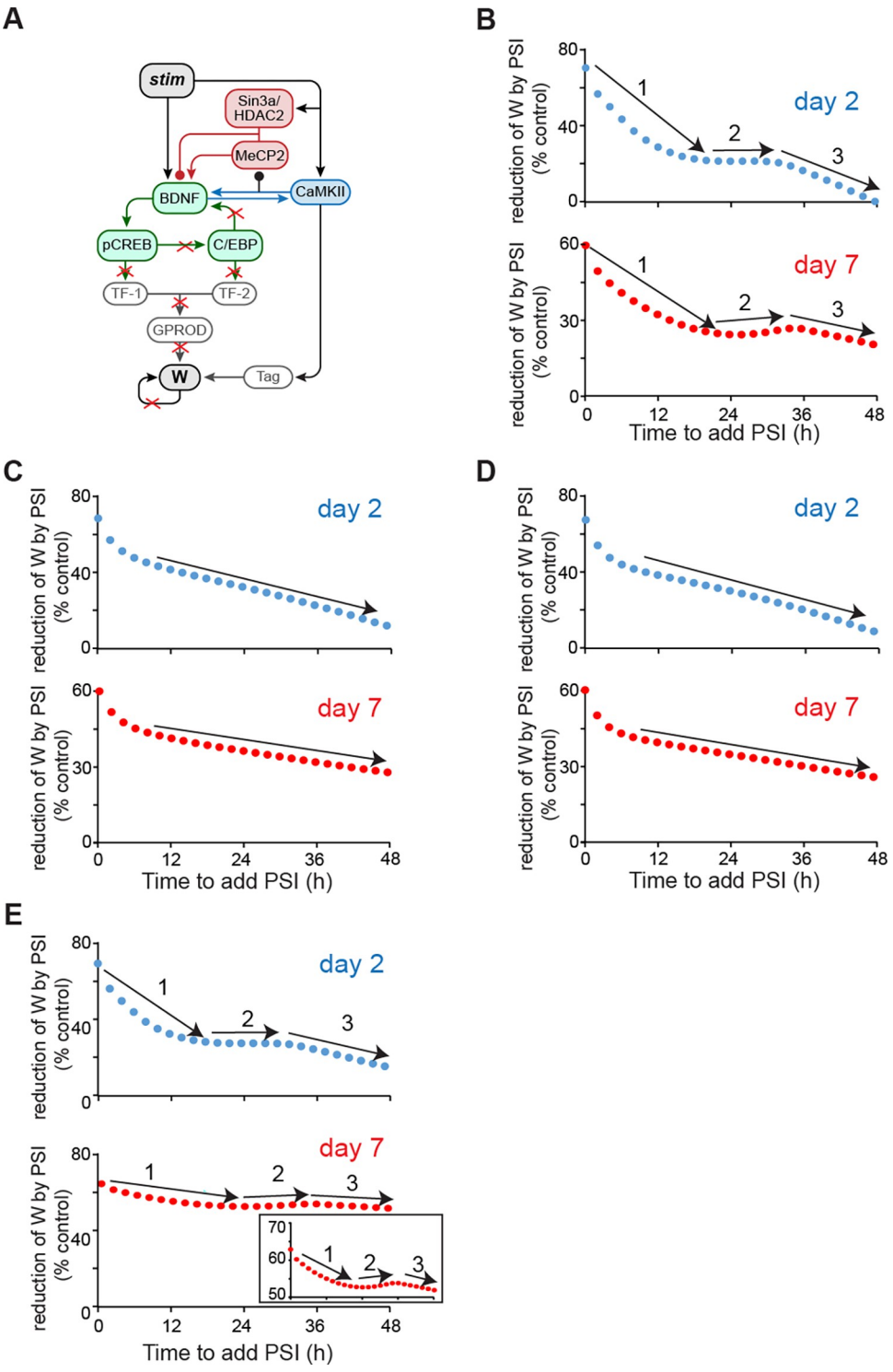

Fig 3. Simulated response to PSI. (A) Schematic model of the pathways that are blocked by PSI (red X's). (B) Reduction of synaptic weight W at day 2 (blue curve) and 7 (red curve) after training, with the addition of PSI initiated at varying times. '1','2','3' represent different phases. (C-D) Simulated reduction of W response to PSI in the absence of the BDNF-CaMKIIα feedback loop (C) or of the BDNF-C/EBPβ feedback loop (D) or of the downstream W loop (E) at day 2 (blue) and day 7 (red). Insert in (E), same as main panel except Y axis scale is expanded to more clearly illustrate vertical variations in W.

https://doi.org/10.1371/journal.pcbi.1010239.g003

addition, PSI was initiated from 0 h to 48 h after the stimulus. The curve of resistance of W in response to PSI (Y axis of Fig 3B) was built by measuring the degree of PSI-induced reduction of W at day 2 or day 7 post-stimulus (Fig 3B). The Y axis of Fig 3B varies from 0% to 100% of the control W in the absence of PSI. If W was reduced to zero, then the reduction was 100%. If W remained intact, then the reduction was 0%. If the attenuation of W in response to PSI decreased, the resistance of W to PSI increased. As expected, early application of PSI was most effective in attenuating W, and the resistance of W to PSI increased with the time of PSI application, leading to an overall decrease in the reduction of W by PSI with time (Fig 3B). However, unexpectedly, the PSI-induced attenuation at day 2 and day 7 did not show a continuous decrease over time, instead displaying multiple phases. During the first phase after stimulus, when PSI was initiated between immediately and 25 h post stimulus, the reduction of W at day 2 and 7 decreased with respect to the time at which PSI was initiated (arrows #1, Fig 3B), corresponding to an increase of resistance. During the second phase, when PSI was initiated between 25 and 35 h post stimulus (arrows #2, Fig 3B), attenuation of W at day 2 remained around the same level (blue curve, Fig 3B), whereas attenuation of W at day 7 increased with respect to the time at which PSI was initiated (red curve, Fig 3B), corresponding to a decrease of resistance. After 35 h post-stimulus, attenuation of W at days 2 and 7 resumed decreasing with respect to the time at which PSI was initiated (arrows #3, Fig 3B). Thus, there is a period of time, between 25 and 35 h post-stimulus, during which the resistance of late W (at 7 days) paradoxically decreases with respect to the time of PSI application. These dynamics predict distinct periods during which memory consolidation is differentially affected with respect to the time of PSI application.

To investigate whether the model can also produce a multi-phased response to other disruptions as it did to PSI, we simulated the effects of anti-BDNF oligodeoxynucleotide (ODN) and anti-C/EBP ODN (S2A Fig). To make the results comparable to PSI treatments, we suppressed 80% of BDNF activity for 6 h to simulate the effects of anti-BDNF ODN (S2A Fig). We suppressed 80% of C/EBPβ activity for 6 h to simulate the effects of anti-C/EBP ODN (S2B Fig). We also simulated the effects of suppressing 80% of MeCP2 activity for 6 h (S2C Fig). We found multiple phases of W reduction in response to all of these treatments, qualitatively similar to those resulting from PSI (S2 Fig). These results suggest that distinct periods of memory resistance to disruptions during memory consolidation may be a general phenomenon, not only a response to PSI.

To test the effects of the BDNF dependent feedback loops on the multiple phases of W reduction in response to PSI, the simulations were repeated, blocking either the BDNF-CaMKIIα feedback loop (Fig 3C) or the BDNF-C/EBPβ feedback loop (Fig 3D). Blocking either feedback loop eliminated the second phase during which the reduction of W did not significantly decrease with the time of PSI, for W at day 2 (Fig 3C and 3D, blue curves) and day 7 (Fig 3C and 3D, red curves). Instead, attenuation of W continuously decreased. Thus, both BDNF dependent feedback loops are necessary for generating multiple phases of W resistance to PSI.

To test the effects of the independent downstream W positive feedback loop on the multiple phases of W resistance in response to PSI, the simulations of Fig 3B were repeated in Fig 3E, blocking the downstream W feedback loop. Blocking this loop enhanced the reduction of W by PSI. However, the three phases of resistance of W in response to PSI were still present (arrows #1, 2, 3, Fig 3E). Thus, this characteristic dynamics of the resistance of W with respect to the time to initiate PSI are not dependent on the downstream W feedback.

The role of dual effects of MeCP2 on expression of BDNF in the complex dynamics of resistance of W in response to PSI

We compared the time courses of model variables, in the presence *vs*. absence of PSI applied at different times, in order to further examine the mechanism underlying the distinct dynamics

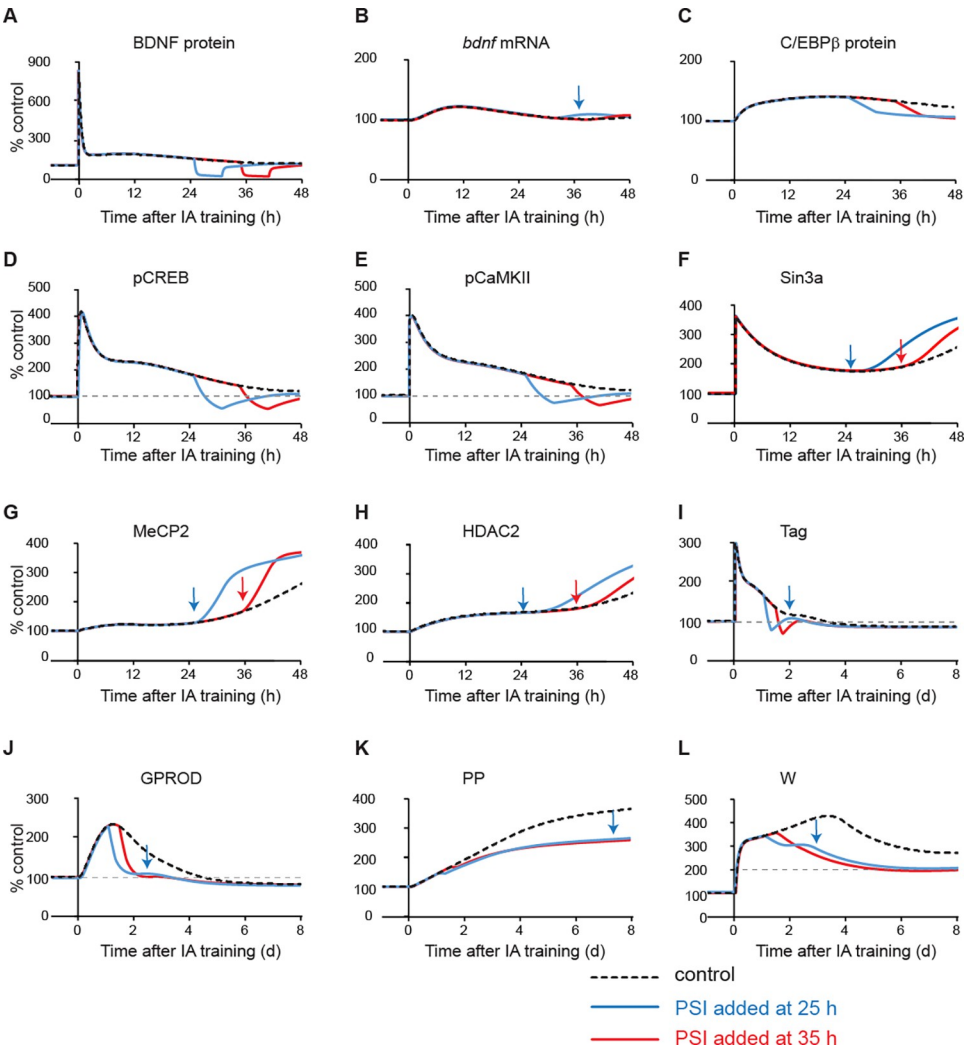

Fig 4. Simulated dynamics of model variables when PSI was added 25 h or 35 h post-stimulus. Example of dynamics of BDNF protein/mRNA (A-B), C/EBPβ protein (C), pCREB (D), pCaMKIIα (E), and Sin3a binding (F), MeCP2 binding (G), HDAC2 binding (H), Tag (I), GROD (J), PP (K), and W (L), without PSI (black dashed) or with PSI added at 25 h post- stimulus (blue), or at 35 h post- stimulus (red).

https://doi.org/10.1371/journal.pcbi.1010239.g004

of W reduction with respect to the time of PSI initiation during the second phase (Fig 4). We selected the time points of 25 h and 35 h post stimulus because these two time points are the beginning and end of the second phase (Fig 3B). Here we investigated why W at day 7 with PSI added at 25 h was greater than W with PSI added at 35 h, (i.e., the reduction of W by PSI applied at 25 h was less than the reduction of W by PSI applied at 35 h). With PSI added 25 or 35 h post stimulus, BDNF decreased in both cases, leading to a decrease in pCaMKIIα (Fig 4A and 4E, blue *vs*. red *vs*. black dashed curves), releasing its inhibitory effect on MeCP2 binding (Fig 4G, blue *vs*. red *vs*. black dashed curves). However, when PSI was added at 25 h, MeCP2 binding quickly increased (Fig 4G, blue arrow), faster than the increase of Sin3a and HDAC2 binding which remained low for several hours before their increase (Fig 4F and 4H, blue arrows). Thus, MeCP2 alone bound to *bdnf* exon IV promoter to increase the expression of *bdnf*, before Sin3a and HDAC2 could bind it to form the inhibitory complex. The increase in *bdnf* expression occurred after PSI was removed, due to the increased binding of MeCP2 alone

(Fig 4B, blue arrow). Translation of excess mRNA generated a late increase of BDNF that enhanced the recovery of the BDNF-dependent feedback loops, including BDNF, pCREB1 and pCaMKIIα (Fig 4A, 4D and 4E, blue curves), which led to a second wave of increase in Tag and GPROD (Fig 4I and 4J, blue arrows). The enhanced Tag and GPROD subsequently increased W and its precursor PP (Fig 4K, blue arrow), with PP initiating the downstream feedback loop, leading to a second wave of increase in W (Fig 4L, blue arrow). In contrast, when PSI was added later, 35 h post-stimulus, Sin3a and HDAC2 binding were already increasing (Fig 4F and 4H, red arrows), so that increased MeCP2 binding was directed more to the MeCP2/Sin3a/HDAC2 complex, repressing *bdnf*. Therefore, no enhanced recovery was induced in any variables (Fig 4A–4L, red curves) and the late increase of W was diminished. Thus, due to the dual effects of MeCP2 on the BDNF-dependent feedback loops, W at day 7 had a paradoxically higher value when PSI was added at 25 h than when PSI was added later at 35 h post-stimulus (Fig 4L, blue *vs*. red curves). These dynamics generate the period within which the resistance of W to PSI decreased with respect to the time of PSI application.

Parameter sensitivity analysis to identify additional factors that affect the complex dynamics of resistance of W in response to PSI

Many pathways are involved in the PSI resistance profile. However, the core components of the model are two BDNF-dependent feedback loops, the MeCP2/Sin3a/HDAC2 complex, and synaptic tagging and capture. All the pathways directly or indirectly modulate these four components. Instead of exhaustively listing the sensitivity of all metrics of model function, we investigated which components are critical for determining the temporal profile of resistance to PSI. Fig 3 suggests that the BDNF-dependent feedback loops are necessary for the multiple phases of W response to PSI. Parameter sensitivity analysis was performed to further examine the extent to which the MeCP2/Sin3a/HDAC2 complex and synaptic tagging and capture might contribute to the dynamics of resistance of W dynamics to PSI (Fig 5). In Fig 5A, τ_{comp}, the time constant for the inhibitory effects of the MeCP2/Sin3a/HDAC2 complex on *bdnf* exon promoter, was reduced to 30% of the standard value in Table 1. The second phase of W reduction was eliminated. In Fig 5B, τ_{E_MeCP2}, the time constant of activating effects of free MeCP2 on *bdnf exon* promoter, was increased to 300% of the standard value in Table 1. The second phase of W reduction was eliminated. Thus, the time scales of the dynamics governing the effects of the MeCP2/Sin3a/HDAC2 complex, and the effects of free MeCP2, played critical roles in the generation of the multiple phases of W reduction in response to PSI. Analogous simulations demonstrated that decreasing τ_{HDAC2} (the time scale of HDAC2 binding to *bdnf*) to 30% of its standard value or enhancing the response of Sin3a binding to stimulus, r_{sin3a}, by 300% eliminated the second phase of W reduction in response to PSI (Fig 5C and 5D).

In Fig 5E, varying τ_{Tag}, the time constant of Tag activation, from 30% to 300% of the standard value, did not substantially change the multiple phases of W reduction in response to PSI. Likewise, in Fig 5F, varying τ_{GPROD}, the time constant of GPROD production, from 30% to 300% of its standard value, also did not substantially change the multiple phases of W reduction in response to PSI. This parameter sensitivity analysis suggests that the variables of the tagging and capture system did not play important roles in the generation of the multiple phases of W reduction in response to PSI. The parameters governing the multiple phases of W reduction are those related to the dynamics of MeCP2, Sin3a and HDAC2 effects on *bdnf* expression.

These simulations also suggest that although BDNF-dependent feedback loops are necessary for the multiple phases of W reduction response to PSI (Fig 3C and 3D), they are not sufficient in the absence of further parameter constraints. The multiple phases of response of W

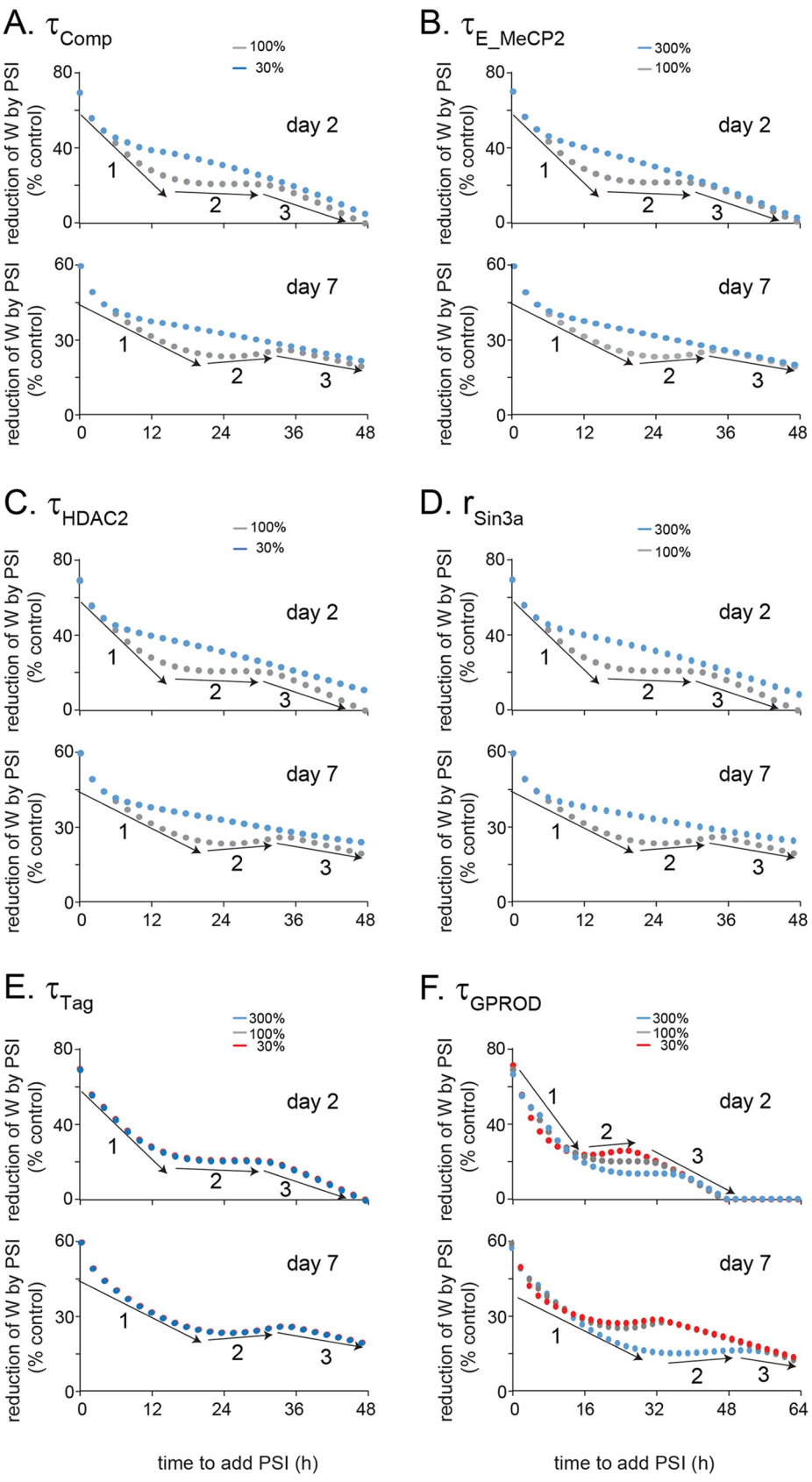
A. τComp
B. τE_MeCP2
C. τHDAC2
D. rSin3a
E. τTag
F. τGPROD
100%
30%
300%
day 2
day 7
reduction of W by PSI (% control)
time to add PSI (h)
1
2
3

Fig 5. Simulated effects of various parameters on the multiple phases of W resistance in response to PSI. The dynamics of reduction of W at day 2 and 7 post-stimulus, with the addition of PSI initiated from 0 h to 48 h, varied when altering τ_{Comp} (A), τ_{E_MeCP2} (B), τ_{HDAC2} (C), r_{Sin3a} (D), τ_{Tag} (E), τ_{GPROD} (F). '1','2','3' represent different phases.

https://doi.org/10.1371/journal.pcbi.1010239.g005

only occur within a specific range of the time constants governing the dynamics of regulation of *bdnf* expression by MeCP2, Sin3a and HDAC2. Thus MeCP2, Sin3a and HDAC2 binding kinetics may constitute potential targets for rescuing memory impaired by disruptions.

Discussion

Empirical studies indicate that recurrent rounds of *de novo* protein synthesis are required to maintain hippocampal memory formation and consolidation for a week or longer [5, 25,26]. However, the ways in which the dynamics of these molecular components of consolidation correlate with different temporal domains of memory is not well understood. BDNF, with levels elevated by feedback, may enhance the expression of downstream proteins such as C/EBP, rendering memory consolidation resistant to disruption during specific post-training periods. In Zhang et al. [3], we developed a differential-equation based model to describe this feedback loop. In the current study, the model of Zhang et al. [3] was revised to further investigate the roles of a BDNF-CREB-C/EBPβ feedback loop and of a BDNF-CaMKIIα dependent feedback loop in the development of resistance to PSI during memory consolidation.

A characteristic feature of a positive feedback loop is that if PSI is not sufficient to reduce the protein synthesis rate to below a threshold for substantial time, then the positive feedback loops will fully recover after PSI is removed [24, 40]. In the model of Zhang et al. [24], after the feedback loops were initiated and the strength grew with time, the resistance of W to PSI was gradually enhanced with time. However, empirical studies suggest that, for some common learning protocols, the resistance of memory to PSI does not continuously increase with the delay in the time to initiate PSI [25–26, 39, 49–51]. In some periods, the resistance decreases with respect to the time of PSI initiation. Because there are too many variables (e.g., type of training, circadian rhythms, age, areas of the brain, animal) to definitively characterize the concept of a time window(s), the data surrounding time windows is too vague and paradigm sensitive. We did not use our model to replicate the time windows found in empirical studies. In this study, we used the revised model to investigate the dynamics of variation of synaptic weight W with respect to the time of PSI. We found multiple phases of W resistance in response to PSI (Fig 3B). The dual effects of MeCP2 on the expression of *bdnf* helped generate a specific period during which the resistance of W at day 7 post-stimulus to PSI decreased with respect to the time of PSI application.

When PSI was added, the synthesis of BDNF was reduced, leading to a decrease of pCaMKIIα, which subsequently increased binding of MeCP2 to the *bdnf* exon *IV* promoter (Fig 4). If binding of MeCP2 increased before the increase of Sin3a and HDAC2 binding, MeCP2 alone increased the expression of *bdnf*, enhancing the ability of the BDNF feedback loops to recover after PSI was removed. In contrast, if binding of MeCP2 to the *bdnf* promoter increased together with increased Sin3a and HDAC2 binding, then the MeCP2/Sin3a/HDAC2 complex would inhibit the expression of *bdnf*, suppressing the ability of BDNF feedback loops to recover after PSI was removed. Thus, the multiple phases of W in response to PSI application depend on the temporal difference in the dynamics of binding of MeCP2, Sin3a and HDAC2, *vs*. binding of MeCP2 alone, to regulate the expression of *bdnf* (Figs 4 and 5). Simulations also suggest that both BDNF-related feedback loops, but not the downstream W feedback, are required for the multiple phases of W resistance in response to PSI (Fig 3). The dependence of these phases of response of W to PSI on the dual regulation of *bdnf* by MeCP2

suggests that the special MeCP2 binding kinetics may provide a possible explanation of complex effects of MeCP2 on gene expression [28–29, 52] and a potential therapeutic target for rescuing memory impaired by disruptions.

Dual regulation of *bdnf* by MeCP2 might also help explain apparent rapid forgetting of infantile memory. Multiple hypotheses have been proposed to explain the mechanism of infantile amnesia and reinstatement of latent memory traces [8, 10, 47,48, 53]. In Travaglia et al. [12], in infantile rats, the basal level of pCaMKIIα in dorsal hippocampus is substantially lower than that of adult rats, whereas the basal level of pCREB in dorsal hippocampus is substantially higher than that of adult. We therefore simulated a stimulus response given a decreased basal phosphorylation rate of pCaMKIIα and increased basal phosphorylation rate of pCREB (Fig 2). Increased pCREB led to an increase of C/EBPβ, tending to augment the BDNF-C/EBPβ feedback loop. However, the decreased pCaMKIIα led to an increased level of the MeCP2/Sin3a/HDAC2 complex, suppressing the BDNF-C/EBPβ feedback loop. The net result of these effects was that although the synaptic weight W post-stimulus transiently increased due to the increase in pCREB, this increase was not sufficient to overcome the suppression of feedback and maintain W at day 7 post-stimulus at a sufficiently high level to retrieve memory (Fig 2B, blue curves). However, W did remain at an elevated level, compared to pre-stimulus baseline, at day 7, suggesting memory reinstatement due to specific protocols may be elicited at later times. The simulation results also help explain why exogenous application of BDNF can restore infantile memory [9]. It is possibly via overcoming the suppression of *bdnf* expression by MeCP2/Sin3a/HDAC2 complex. Multiple signaling cascades in addition to those modeled here are involved in infantile amnesia [54] (e.g., changes in glutamate receptor composition [9, 55]). It is not currently possible to quantitively or qualitatively assign a relative importance to any of these changes individually or in combination. The data are insufficient at this time to make such a specific determination. Here, we have offered a first step toward addressing this issue by developing a model that simulates aspects of infantile amnesia as well as other dynamic features of memory consolidation, such as its susceptibility to protein synthesis inhibition. We chose to focus on dynamics of pCaMKIIα and pCREB for two reasons. First, empirical studies have measured the time courses of on pCaMKIIα and pCREB activation after IA training in adult rats [5]. Second, significant differences in pCaMKIIα and pCREB basal activities have been found between infant and adult rats [12], which provide data for model simulations. These simulations suggest that in infant animals, decreased basal CaMKIIα activity and increased basal levels of bound MeCP2/Sin3a/HDAC2 complex may contribute to fast forgetting of infantile memory in the early phase. As more data become available, models such as our will be a valuable tool in evaluating the complex and dynamic features of memory and the ways in which specific neuronal processes contribute to memory.

The model is of a single compartment. We did not model subcellular or separate synaptic compartments. We note that kinases (e.g., CaMKIIα) in different compartments might have differential contributions to long-term synaptic plasticity, and the contribution of synaptic tagging and capture may also differ based on the area of brain region involved in memory consolidation [56,57]. However, a single compartment model has the advantage of reducing the number of parameters, avoiding the introduction of a large number of relatively poorly constrained, compartment-specific parameters. Therefore, our analyses and model are simplified and focus on the activating roles of kinases and on synaptic tagging and capture in the induction and consolidation long-term synaptic potentiation. We will, however, evaluate on an ongoing basis whether a multi-compartment model would be likely to improve predictions.

Although the revised model is based on some relatively speculative assumptions, several predictions can be derived from the present simulations. First, for adult rats, the simulations predict critical roles of MeCP2 in helping to delineate the multiple phases of resistance of W to

PSI. Second, for adult rats, the model also predicts ways in which the dynamics of W and other variables would be altered by changing kinetics of the BDNF-related feedback loops, or binding of the transcription factors MeCP2, Sin3a, or HDAC2 to the *bdnf exon* promoter. Finally, for infant rats, the model also predicts that decreased activation of CaMKIIα, combined with increased MeCP2/Sin3a/HDAC2 binding, underlies in part the rapid forgetting of infantile memory. If these predictions can be validated by empirical studies, they may suggest paths towards novel potential therapeutic targets for rescuing memory impairment.

Besides infantile amnesia, signaling pathways in the model (e.g., BDNF, CREB, HDAC, synaptic tagging and capture) are directly or indirectly involved in memory forgetting under various situations, such as aging, sleep deprivation, or aberrant protein degradation [58–62]. To simulate altered dynamics of model components in these situations might also suggest novel methods to rescue memory deficits. For example, CREB and BDNF levels are decreased in sleep deprived mice [60], which would tend to suppress BDNF-dependent feedback loops after training. Based on this, we predict that an inhibitor of MeCP2/Sin3a/HDAC2 complex formation or activity might help to overcome effects of reduced CREB and BDNF due to sleep deprivation, and activate BDNF-dependent feedback loops to restore long-term memory.

Supporting information

S1 Fig. Simulated effects of increased pCREB combined with decreased pCaMKIIα on bistability. (A1) Modification of model. Increased basal phosphorylation of CREB k_{basalp_creb}, concurrent with decreased basal phosphorylation of CaMKIIα k_{basalp_CaMKII}, in the absence of the effects of MeCP2/HDAC2/Sin3a (red) ($[E_{comp}] = 0$; $[E_{MeCP2}] = 0$). (B) Example of dynamics of BDNF protein/mRNA (B1-2), C/EBPβ protein (B3), pCREB (B4), and pCaMKIIα (B5) after training in the presence (black dashed) or absence (blue) of the effects of MeCP2/HDAC2/Sin3a. In the absence of MeCP2/HDAC2/Sin3a inhibitory complex, the variables were switched to a higher steady states after training (blue). However, decreasing k_{basalp_CaMKII} by ~50% blocked the bistable switch (red). (C) Summary table. The steady states of variables 48 h after training with k_{basalp_creb} increasing from the standard value in Table 1 to ~300% of the standard value, and k_{basalp_CaMKII} decreasing from the standard value in Table 1 to 10% of the standard value.
(TIF)

S2 Fig. Simulated response to memory disruptors. (A) Reduction of synaptic weight W at day 2 (blue curve) and 7 (red curve) after training, with the addition of anti-BDNF ODN initiated at varying times. (B) Reduction of synaptic weight W at day 2 (blue curve) and 7 (red curve) after training, with the addition of anti-C/EBP ODN initiated at varying times. (C) Reduction of synaptic weight W at day 2 (blue curve) and 7 (red curve) after training, with the addition of MeCP2 inhibitor initiated at varying times. '1','2','3' represent different phases.
(TIF)

Author Contributions

Conceptualization: Yili Zhang, Paul Smolen, Cristina M. Alberini, Douglas A. Baxter, John H. Byrne.

Data curation: Yili Zhang.

Formal analysis: Yili Zhang.

Funding acquisition: John H. Byrne.

Investigation: Yili Zhang.

Methodology: Yili Zhang, Paul Smolen, Douglas A. Baxter.

Project administration: John H. Byrne.

Software: Yili Zhang.

Supervision: Paul Smolen, Cristina M. Alberini, Douglas A. Baxter, John H. Byrne.

Validation: Yili Zhang, Cristina M. Alberini.

Writing – original draft: Yili Zhang.

Writing – review & editing: Yili Zhang, Paul Smolen, Cristina M. Alberini, Douglas A. Baxter, John H. Byrne.

References

1. Abel T, Lattal KM. Molecular mechanisms of memory acquisition, consolidation and retrieval. Curr. Opin. Neurobiol. 2001; 11: 180–187. https://doi.org/10.1016/s0959-4388(00)00194-x PMID: 11301237
2. Madsen HB, Kim JH. Ontogeny of memory: an update on 40 years of work on infantile amnesia. Behav. Brain Res. 2016; 298: 4–14. https://doi.org/10.1016/j.bbr.2015.07.030 PMID: 26190765
3. Zhang Y, Smolen P, Alberini CM, Baxter DA, Byrne JH. Computational model of a positive BDNF feedback loop in hippocampal neurons following inhibitory avoidance training. Learn. Mem. 2016; 23: 714–722. https://doi.org/10.1101/lm.042044.116 PMID: 27918277
4. Chen DY, Bambah-Mukku D, Pollonini G, Alberini CM. Glucocorticoid receptors recruit the CaMKIIα-BDNF-CREB pathways to mediate memory consolidation. Nat. Neurosci. 2012; 15: 1707–1714. https://doi.org/10.1038/nn.3266 PMID: 23160045
5. Bambah-Mukku D, Travaglia A, Chen DY, Pollonini G, Alberini CM. A positive autoregulatory BDNF feedback loop via C/EBPβ mediates hippocampal memory consolidation. J. Neurosci. 2014; 34: 12547–12559. https://doi.org/10.1523/JNEUROSCI.0324-14.2014 PMID: 25209292
6. Harward SC, Hedrick NG, Hall CE, Parra-Bueno P, Milner TA, Pan E, et al. Autocrine BDNF-TrkB signalling within a single dendritic spine. Nature 2016; 538: 99–103. https://doi.org/10.1038/nature19766 PMID: 27680698
7. Li W, Pozzo-Miller L. BDNF deregulation in Rett syndrome. Neuropharmacology 2014; 76 Pt C(0 0): 737–746. https://doi.org/10.1016/j.neuropharm.2013.03.024 PMID: 23597512
8. Li S, Callaghan BL, Richardson R. Infantile amnesia: forgotten but not gone. Learn. Mem. 2014; 21: 135–139. https://doi.org/10.1101/lm.031096.113 PMID: 24532837
9. Travaglia A, Bisaz R, Sweet ES, Blitzer RD, Alberini CM. Infantile amnesia reflects a developmental critical period for hippocampal learning. Nat. Neurosci. 2016; 19: 1225–1233. https://doi.org/10.1038/nn.4348 PMID: 27428652
10. Guskjolen A, Kenney JW, de la Parra J, Yeung BA, Josselyn SA, Frankland PW. Recovery of "lost" infant memories in mice. Curr. Biol. 2018; 28: 2283–2290.e3. https://doi.org/10.1016/j.cub.2018.05.059 PMID: 29983316
11. Bessières B, Travaglia A, Mowery TM, Zhang X, Alberini CM. Early life experiences selectively mature learning and memory abilities. Nat. Commun. 2020; 11: 628. https://doi.org/10.1038/s41467-020-14461-3 PMID: 32005863
12. Travaglia A, Bisaz R, Cruz E, Alberini CM. Developmental changes in plasticity, synaptic, glia and connectivity protein levels in rat dorsal hippocampus. Neurobiol. Learn. Mem. 2016; 135: 125–138. https://doi.org/10.1016/j.nlm.2016.08.005 PMID: 27523749
13. Bhalla US, Iyengar R. Emergent properties of networks of biological signaling pathways. Science 1999; 283: 381–387. https://doi.org/10.1126/science.283.5400.381 PMID: 9888852
14. Aslam N, Shouval HZ. Regulation of cytoplasmic polyadenylation can generate a bistable switch. BMC Syst. Biol. 2012; 6: 12. https://doi.org/10.1186/1752-0509-6-12 PMID: 22335938
15. Lisman J, Schulman H, Cline H. The molecular basis of CaMKII function in synaptic and behavioural memory. Nat. Rev. Neurosci. 2002; 3: 175–190. https://doi.org/10.1038/nrn753 PMID: 11994750
16. Liu RY, Fioravante D, Shah S, Byrne JH. cAMP response element-binding protein 1 feedback loop is necessary for consolidation of long-term synaptic facilitation in *Aplysia*. J. Neurosci. 2008; 28: 1970–1976. https://doi.org/10.1523/JNEUROSCI.3848-07.2008 PMID: 18287513

17. Kotaleski JH, Blackwell KT. Modelling the molecular mechanisms of synaptic plasticity using systems biology approaches. Nat. Rev. Neurosci. 2010; 11: 239–251. https://doi.org/10.1038/nrn2807 PMID: 20300102

18. Ogasawara H, Kawato M. Bistable switches for synaptic plasticity. Sci. Signal. 2009; 2: pe7. https://doi.org/10.1126/scisignal.256pe7 PMID: 19193606

19. Pettigrew DB, Smolen P, Baxter DA, Byrne JH. Dynamic properties of regulatory motifs associated with induction of three temporal domains of memory in *Aplysia*. J. Comput. Neurosci. 2005; 18: 163–181. https://doi.org/10.1007/s10827-005-6557-0 PMID: 15714268

20. Shema R, Sacktor TC, Dudai Y. Rapid erasure of long-term memory associations in the cortex by an inhibitor of PKMζ. Science 2007; 317: 951–953. https://doi.org/10.1126/science.1144334 PMID: 17702943

21. Smolen P, Baxter DA, Byrne JH. Molecular constraints on synaptic tagging and maintenance of long-term potentiation: a predictive model. PLoS Comput. Biol. 2012; 8: e1002620. https://doi.org/10.1371/journal.pcbi.1002620 PMID: 22876169

22. Smolen P, Baxter DA, Byrne JH. How can memories last for days, years, or a lifetime? Proposed mechanisms for maintaining synaptic potentiation and memory. Learn. Mem. 2019; 26: 133–150. https://doi.org/10.1101/lm.049395.119 PMID: 30992383

23. Zhang F, Endo S, Cleary LJ, Eskin A, Byrne JH. Role of transforming growth factorβ in long-term synaptic facilitation in *Aplysia*. Science 1997; 275: 1318–1320. https://doi.org/10.1126/science.275.5304.1318 PMID: 9036859

24. Zhang Y, Smolen P, Baxter DA, Byrne JH. The sensitivity of memory consolidation and reconsolidation to inhibitors of protein synthesis and kinases: computational analysis. Learn. Mem. 2010; 17: 428–439. https://doi.org/10.1101/lm.1844010 PMID: 20736337

25. Bekinschtein P, Cammarota M, Igaz LM, Bevilaqua LR, Izquierdo I, Medina JH. Persistence of long-term memory storage requires a late protein synthesis- and BDNF-dependent phase in the hippocampus. Neuron 2007; 53: 261–277. https://doi.org/10.1016/j.neuron.2006.11.025 PMID: 17224407

26. Bourtchouladze R, Abel T, Berman N, Gordon R, Lapidus K, Kandel ER. Different training procedures recruit either one or two critical periods for contextual memory consolidation, each of which requires protein synthesis and PKA. Learn. Mem. 1998; 5: 365–374. PMID: 10454361

27. Raven F, Bolsius YG, van Renssen LV, Meijer EL, van der Zee EA, Meerlo P, et al. Elucidating the role of protein synthesis in hippocampus-dependent memory consolidation across the day and night. Eur. J. Neurosci. 2021; 54: 6972–6981. https://doi.org/10.1111/ejn.14684 PMID: 31965655

28. Ibrahim A, Papin C, Mohideen-Abdul K, Le Gras S, Stoll I, Bronner C, et al. MeCP2 is a microsatellite binding protein that protects CA repeats from nucleosome invasion. Science 2021; 372: eabd5581. https://doi.org/10.1126/science.abd5581 PMID: 34324427

29. Sharifi O, Yasui DH. The molecular functions of MeCP2 in Rett syndrome pathology. Front Genet. 2021; 12: 624290. https://doi.org/10.3389/fgene.2021.624290 PMID: 33968128

30. Abuhatzira L, Makedonski K, Kaufman Y, Razin A, Shemer R. MeCP2 deficiency in the brain decreases BDNF levels by REST/CoREST-mediated repression and increases TrkB production. Epigenetics 2007; 2: 214–222. https://doi.org/10.4161/epi.2.4.5212 PMID: 18075316

31. Chahrour M, Jung SY, Shaw C, Zhou X, Wong ST, Qin J, et al. MeCP2, a key contributor to neurological disease, activates and represses transcription. Science 2008; 320: 1224–1229. https://doi.org/10.1126/science.1153252 PMID: 18511691

32. Chen WG, Chang Q, Lin Y, Meissner A, West AE, Griffith EC, et al. Derepression of BDNF transcription involves calcium-dependent phosphorylation of MeCP2. Science 2003; 302: 885–889. https://doi.org/10.1126/science.1086446 PMID: 14593183

33. Martinowich K, Hattori D, Wu H, Fouse S, He F, Hu Y, et al. DNA methylation-related chromatin remodeling in activity-dependent BDNF gene regulation. Science 2003; 302: 890–893. https://doi.org/10.1126/science.1090842 PMID: 14593184

34. Smolen P, Wood MA, Baxter DA, Byrne JH. Modeling suggests combined-drug treatments for disorders impairing synaptic plasticity via shared signaling pathways. J. Comput. Neurosci. 2020; https://doi.org/10.1007/s10827-020-00771-4 PMID: 33175283

35. Frey U, Morris RG. Synaptic tagging and long-term potentiation. Nature. 1997; 385: 533–536. https://doi.org/10.1038/385533a0 PMID: 9020359

36. Moncada D, Viola H. Induction of long-term memory by exposure to novelty requires protein synthesis: evidence for a behavioral tagging. J Neurosci. 2007; 27: 7476–7481. https://doi.org/10.1523/JNEUROSCI.1083-07.2007 PMID: 17626208

37. Ballarini F, Moncada D, Martinez MC, Alen N, Viola H. Behavioral tagging is a general mechanism of long-term memory formation. Proc. Natl. Acad. Sci. U S A. 2009; 106: 14599–14604. https://doi.org/10.1073/pnas.0907078106 PMID: 19706547

38. Moncada D, Ballarini F, Martinez MC, Frey JU, Viola H. Identification of transmitter systems and learning tag molecules involved in behavioral tagging during memory formation. Proc. Natl. Acad. Sci. U S A. 2011; 108: 12931–12936. https://doi.org/10.1073/pnas.1104495108 PMID: 21768371

39. Slipczuk L, Bekinschtein P, Katche C, Cammarota M, Izquierdo I, Medina JH. BDNF activates mTOR to regulate GluR1 expression required for memory formation. PLoS One. 2009; 4: e6007. https://doi.org/10.1371/journal.pone.0006007 PMID: 19547753

40. Milekic MH, Brown SD, Castellini C, Alberini CM. Persistent disruption of an established morphine conditioned place preference. J. Neurosci. 2006; 26: 3010–3020. https://doi.org/10.1523/JNEUROSCI.4818-05.2006 PMID: 16540579

41. Taubenfeld SM, Milekic MH, Monti B, Alberini CM. The consolidation of new but not reactivated memory requires hippocampal C/EBPβ. Nat. Neurosci. 2001; 4: 813–818. https://doi.org/10.1038/90520 PMID: 11477427

42. Lisman JE, Goldring MA. Feasibility of long-term storage of graded information by the Ca^{2+}/calmodulin-dependent protein kinase molecules of the postsynaptic density. Proc. Natl. Acad. Sci. 1988; 85: 5320–5324. https://doi.org/10.1073/pnas.85.14.5320 PMID: 3393540

43. Boggio EM, Lonetti G, Pizzorusso T, Giustetto M. Synaptic determinants of Rett syndrome. Front. Synaptic. Neurosci. 2010 Aug 6. 2: 28. https://doi.org/10.3389/fnsyn.2010.00028 eCollection 2010. PMID: 21423514

44. Smolen P, Baxter DA, Byrne JH. A model of the roles of essential kinases in the induction and expression of late long-term potentiation. Biophys. J. 2006; 90: 2760–2675. https://doi.org/10.1529/biophysj.105.072470 PMID: 16415049

45. Ermentrout B. Simulating, analyzing, and animating dynamical systems: A guide to XPPAUTO for researchers and students. SIAM, Philadelphia, USA. 2002.

46. McDougal RA, Morse TM, Hines ML, Shepherd GM. ModelView for ModelDB: online presentation of model structure. Neuroinformatics. 2015; 13: 459–470. https://doi.org/10.1007/s12021-015-9269-2 PMID: 25896640

47. Josselyn SA, Frankland PW. Infantile amnesia: a neurogenic hypothesis. Learn. Mem. 2012; 19: 423–433. https://doi.org/10.1101/lm.021311.110 PMID: 22904373

48. Tsai TC, Huang CC, Hsu KS. Infantile amnesia is related to developmental immaturity of the maintenance mechanisms for long-term potentiation. Mol. Neurobiol. 2019; 56: 907–919. https://doi.org/10.1007/s12035-018-1119-4 PMID: 29804230

49. Grecksch G, Matthies H. Two sensitive periods for the amnesic effect of anisomycin. Pharmacol. Biochem. Behav. 1980; 12: 663–665. https://doi.org/10.1016/0091-3057(80)90145-8 PMID: 7393961

50. Tiunova AA, Anokhin KV, Rose SP. Two critical periods of protein and glycoprotein synthesis in memory consolidation for visual categorization learning in chicks. Learn. Mem. 1998; 4: 401–410. https://doi.org/10.1101/lm.4.5.401 PMID: 10701879

51. Igaz LM, Vianna MR, Medina JH, Izquierdo I. Two time periods of hippocampal mRNA synthesis are required for memory consolidation of fear-motivated learning. J. Neurosci. 2002; 22: 6781–6789.

52. Zhou J, Zoghbi H. Repeat after Me(CP2)! Science 2021; 372: 1390–1391.

53. Alberini CM, Travaglia A. Infantile amnesia: a critical period of learning to learn and remember. J. Neurosci. 2017; 37: 5783–5795. https://doi.org/10.1523/JNEUROSCI.0324-17.2017 PMID: 28615475

54. Callaghan BL, Li S, Richardson R. The elusive engram: what can infantile amnesia tell us about memory? Trends Neurosci. 2014; 37: 47–53. https://doi.org/10.1016/j.tins.2013.10.007 PMID: 24287309

55. Tsai TC, Huang CC, Hsu KS. Infantile amnesia is related to developmental immaturity of the maintenance mechanisms for long-term potentiation. Mol. Neurobiol. 56: 907–919. https://doi.org/10.1007/s12035-018-1119-4 PMID: 29804230

56. Pavlowsky A, Alarcon JM. Interaction between long-term potentiation and depression in CA1 synapses: temporal constrains, functional compartmentalization and protein synthesis. PLoS One. 2012; 7: e29865. https://doi.org/10.1371/journal.pone.0029865 PMID: 22272255

57. Sajikumar S, Navakkode S, Frey JU. Identification of compartment- and process-specific molecules required for "synaptic tagging" during long-term potentiation and long-term depression in hippocampal CA1. J. Neurosci. 2007; 27: 5068–5080. https://doi.org/10.1523/JNEUROSCI.4940-06.2007 PMID: 17494693

58. Wong LW, Chong YS, Lin W, Kisiswa L, Sim E, Ibáñez CF, Sajikumar S. Age-related changes in hippocampal-dependent synaptic plasticity and memory mediated by p75 neurotrophin receptor. Aging Cell. 2021; 20: e13305. https://doi.org/10.1111/acel.13305 PMID: 33448137

59. Wong LW, Chong YS, Wong WLE, Sajikumar S. Inhibition of histone deacetylase reinstates hippocampus-dependent long-term synaptic plasticity and associative memory in sleep-deprived mice. Cereb. Cortex. 2020; 30: 4169–4182. https://doi.org/10.1093/cercor/bhaa041 PMID: 32188968

60. Wong LW, Tann JY, Ibanez CF, Sajikumar S. The p75 neurotrophin receptor is an essential mediator of impairments in hippocampal-dependent associative plasticity and memory induced by sleep deprivation. J. Neurosci. 2019; 39: 5452–5465. https://doi.org/10.1523/JNEUROSCI.2876-18.2019 PMID: 31085607

61. Navakkode S, Gaunt JR, Pavon MV, Bansal VA, Abraham RP, Chong YS, Ch'ng TH, Sajikumar S. Sex-specific accelerated decay in time/activity-dependent plasticity and associative memory in an animal model of Alzheimer's disease. Aging Cell. 2021; 20: e13502. https://doi.org/10.1111/acel.13502 PMID: 34796608

62. Krishna- K K, Baby N, Raghuraman R, Navakkode S, Behnisch T, Sajikumar S. Regulation of aberrant proteasome activity re-establishes plasticity and long-term memory in an animal model of Alzheimer's disease. FASEB J. 2020; 34: 9466–9479. https://doi.org/10.1096/fj.201902844RR PMID: 32459037